Hindawi
Mathematical Problems in Engineering
Volume 2019, Article ID 8925687, 6 pages
https://doi.org/10.1155/2019/8925687

Research Article

Saddle-Node Bifurcation and Homoclinic Persistence in AFMs with Periodic Forcing

Alexánder Gutiérrez Gutiérrez, Daniel Cortés Zapata, and Diego Alexánder Castro Guevara

Universidad Tecnológica de Pereira (UTP), Pereira, Colombia

Correspondence should be addressed to Daniel Cortés Zapata; danielcorteszapata@utp.edu.co

Received 15 April 2019; Revised 21 July 2019; Accepted 30 July 2019; Published 20 August 2019

Academic Editor: Antonio Elipe

We study the dynamics of an atomic force microscope (AFM) model, under the Lennard-Jones force with nonlinear damping and harmonic forcing. We establish the bifurcation diagrams for equilibria in a conservative system. Particularly, we present conditions that guarantee the local existence of saddle-node bifurcations. By using the Melnikov method, the region in the space parameters where the homoclinic orbits persist is determined in a nonconservative system.

1. Introduction

Atomic force microscopes (AFMs) were developed in 1986 by Bining and coworkers [1]. They are based on the tunneling microscope and the needle profilometer principles. Generally, AFMs measure the interactions between particles, thus allowing the nanoscale study of the surfaces for different materials [2–4]. In fact, a wide variety of applications in the analysis of pharmaceutical products, the study of the properties of fluids and fluids in cellular detection, and studies on medicines, among others, can be found in [5–8].

In the model presented in [9, 10], the authors study the interaction between the sample and the device's tip (Figure 1). The associated differential equation is

$$\ddot{y} + \frac{C}{(y+a)^3}\dot{y} + y = \frac{b_1}{(y+a)^8} - \frac{b_2}{(y+a)^2} + f(t), \tag{1}$$

where b_1, b_2, and a are positive constants and f is a continuous T-periodic function with zero average; that is, $\overline{f} = (1/T)\int_0^T f(t)dt = 0$.

$$F_{\mathrm{LJ}} := \frac{b_1}{(y+a)^8} - \frac{b_2}{(y+a)^2}, \tag{2}$$

where F_{LJ} is known as the Lennard-Jones force, which can be considered as a simple mathematical model to explain the interaction between a pair of neutral atoms or molecules (see [11, 12] for the standard formulation). The first term describes the short-range repulsive force due to overlapping electron orbits, known as Pauli's repulsion, whereas the second term simulates the long-range attraction due to van der Waals' forces. This is a special case of a wide family of Mie forces:

$$F_{n,m}(x) = \frac{A}{x^n} - \frac{B}{x^m}, \tag{3}$$

where n and m are positive integers with $n > m$, also known as the $n-m$ Lennard-Jones force [13]. On the contrary, the dissipative term of (1)

$$F_r = \frac{C}{(y+a)^3}\dot{y}, \tag{4}$$

is associated with a damping force of compression squeeze-film type. In specialized literature, compression film type damping can be considered as the most common and dominant dissipation in different mechanisms (see [14, 15] and their bibliography).

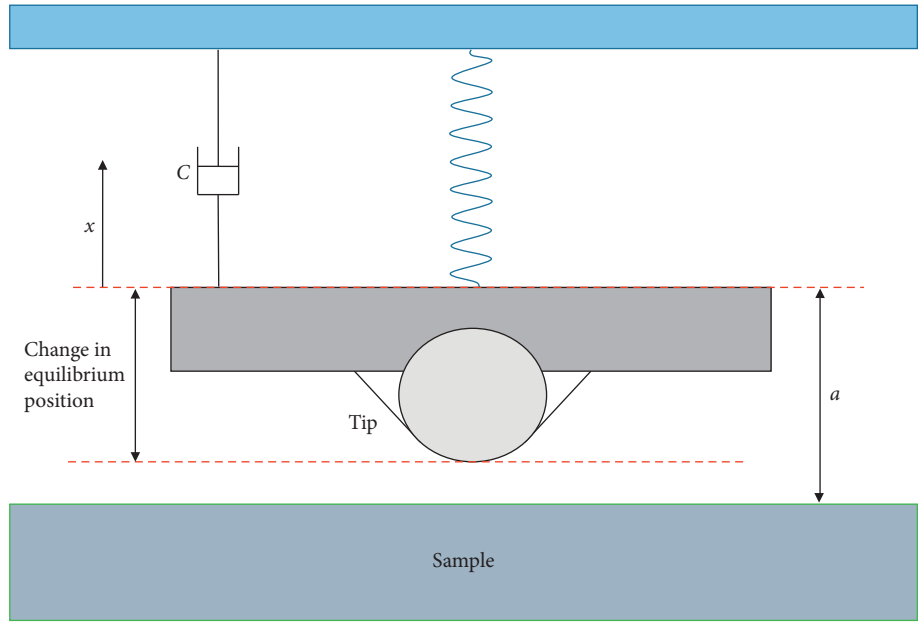

Figure 1: Mechanical model associated with the AFM's devices.

For the conservative system, two main results were obtained, Theorems 1 and 2, where we establish analytically the bifurcation diagram of the equilibria for specific regions with the involved parameters in contrast to the one obtained in [16]. In particular, Theorem 2 proves the local existence of two saddle-node bifurcations that can be related to the hysteresis phenomenon [17, 18].

In the nonconservative system, we present as a main result Theorem 4, which gives a thorough and rigorous condition for the persistence of homoclinic orbit when the external forcing is of the form $f(t) = B\cos(\Omega t)$. The condition found relates the amplitude of the external forcing B with the damping constant C, which in practice can be used to prevent the AFM device from becoming decalibrated.

This article is structured in the following way: Section 1 is an introduction, Section 2 is dedicated to prove the main results in the conservative system, and Section 3 contains the proof for the main result of the nonconservative system along with some illustrative examples.

2. Bifurcation Diagrams

With the change of variable $x = y + a$, (1) is rewritten as

$$\ddot{x} = m(x) + a + \varepsilon\left(f(t) - \frac{C}{x^3}\dot{x}\right), \tag{5}$$

where $m(x) = (b_1/x^8) - x - (b_2/x^2)$ is the total force acting over the system, which is a combination of the Lennard-Jones force and the restoring force of the oscillator. The change of the singularity from $-a$ to 0 will facilitate the study of the bifurcation diagram for equilibria in the conservative system ($\varepsilon = 0$). Note that the classification of the equilibrium solutions of (5) plays an important role when the full equation is studied. We now describe some properties of the function $m(x)$:

$$\lim_{x\longrightarrow 0^+} m(x) = \infty,$$
$$\lim_{x\longrightarrow \infty} \frac{m(x)}{x} = -1. \tag{6}$$

Moreover, m has only one positive root, and a direct analysis provides a critical value

$$b_1^* = \frac{4}{27}b_2^3, \tag{7}$$

such that

(i) If $b_1 > b_1^*$, then $m(x)$ is decreasing

(ii) If $b_1 = b_1^*$, then $m(x)$ is nonincreasing and has an inflection point in $x_c = ((4/3)b_2)^{1/3}$

(iii) Finally, if $b_1 < b_1^*$, then $m(x)$ has a local maximum (resp., minimum) in x_r (resp., x_l) and $m(x_r)$, $m(x_l) < 0$

Therefore, the equilibrium set $\mathcal{G} = \{x \in \mathbb{R}^+ : m(x) + a = 0\}$ is finite, not empty, and the number of equilibria depends on the parameter a. Figure 2 shows the possible variants of the m function in terms of b_1, b_2, and a.

The proof of Theorem 1 will be made by establishing the equilibria for system (5). Let us define the energy function be

$$E(x, v) := \frac{v^2}{2} + \frac{x^2}{2} + \frac{1}{7}\frac{b_1}{x^7} - \frac{b_2}{x} - ax. \tag{8}$$

Note that the local minimums of E correspond to nonlinear centers and the local maximums correspond to saddles. However, when E has a degenerate critical point $(x^*, 0)$, since the Hessian matrix A is such that $\operatorname{Tr} A = 0$, $\operatorname{Det} A = 0$, but $A \neq 0$. In this case, Andronov et al. [19] showed that the system can be written in the "normal" form:

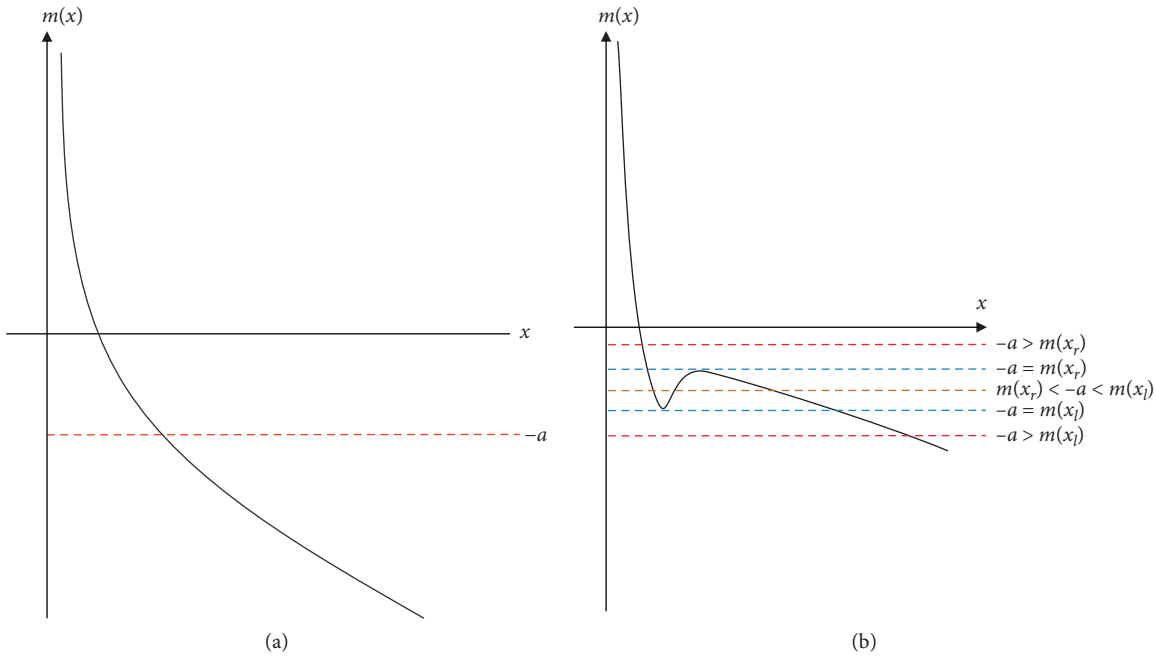

(a) (b)

FIGURE 2: The m function in terms of parameters b_1 and b_2. (a) m is decreasing monotonously if $b_1 > b_1^*$. (b) m has a maximum and a local minimum if $b_1 < b_1^*$.

$$\begin{aligned} \dot{x} &= y, \\ \dot{y} &= a_k x^k [1 + h(x)] + b_n x^n y [1 + g(x)] + y^2 R(x, y), \end{aligned} \tag{9}$$

where $h(x), g(x)$, and $R(x, y)$ are analytic in a neighborhood of the equilibrium point $h(x^*) = g(x^*) = 0$, $k \geq 2$, $a_k \neq 0$, and $n \geq 1$. Thus, the degenerate critical point $(x^*, 0)$ is either a focus, a center, a node, a (topological) saddle, a saddle-node, a cup, or a critical point with an elliptic domain (see [20], Theorem 2, pp. 151; Theorem 3, pp. 151).

Theorem 1. *The equilibrium solutions of the conservative system associated with (5) are classified as follows:*

(1) *A nonlinear center if either* $b_1 \geq b_1^*$ *and* $a \in \mathbb{R}^+$ *or* $b_1 < b_1^*$ *and* $a \in \{\mathbb{R}^+ -] - m(x_r), -m(x_l)[\}$

(2) *Two nonlinear centers and a saddle if* $b_1 < b_1^*$ *and* $a \in] - m(x_r), -m(x_l)[$

(3) *A nonlinear center and a cusp if either* $b_1 < b_1^*$ *and* $a = -m(x_r)$ *or* $a = -m(x_l)$

Proof. We present here the main steps $1 - 3$ of the argument:

(1) Note that $\mathcal{G}$ has a unique element if either $b_1 > b_1^*$ and $a \in \mathbb{R}^+$ or $b_1 < b_1^*$ and $a \in \mathbb{R}^+ -] - m(x_r), -m(x_l)[$, and the equilibrium is a nonlinear center since E reaches a local minimum at that point. For the case $b_1 = b_1^*$, $a = -m(x_c)$ is degenerate, and using the expansion given in (9), we have $k = 3$ and

$$a_k = \frac{24 b_2}{6 x_c^5} - \frac{720 b_1^*}{6 x_c^{11}} < 0. \tag{10}$$

Therefore, from Theorem 2 (pp. 151) of [20], this completes (1).

(2) Under the hypothesis made, the set $\mathcal{G}$ has three solutions such that two are local minimums of E and the other is a local maximum of E. Consequently, two of the equilibria are nonlinear centers and the other equilibrium is a saddle.

(3) In this case, $\mathcal{G}$ has two solutions such that one of them is a local minimum of E and corresponds to a nonlinear center while the other is degenerate with $k = 2$ and $b_1 = 0$ in (9). Consequently, Perko ([20], Theorem 3, pp 151) guarantees that equilibrium is a cusp. □

In the next section, we focus on the persistence of homoclinic orbits present in Theorem 1 when studying equation (5).

The conservative equation associated with (5) can be written as the parametric system:

$$\begin{aligned} x' &= y, \\ y' &= F(x, a), \end{aligned} \tag{11}$$

where $F(x, a) = m(x) + a$. Note that Theorem 1 allows us to build the bifurcation diagram of equilibria in terms of the parameter a (Figures 2 and 3). Moreover, when $b_1 \geq b_1^*$, the parameter a does not modify the dynamics of the system as it

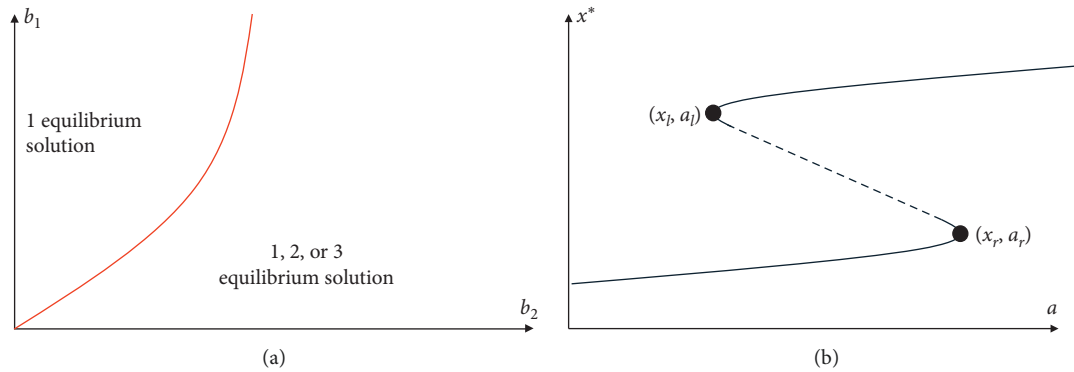

FIGURE 3: Bifurcation diagrams of equation (5) in the conservative system. (a) Bifurcation diagram in terms of the parameters b_1 and b_2. (b) Bifurcation diagram in terms of the parameter a and the number of equilibrium solutions when setting b_1 and b_2 such that $b_1 < b_1^*$.

does when $b_1 < b_1^*$. In fact, there exists numerical evidence [10, 14], which shows that the points (x_i, a_i), with $a_i = -m(x_i)$, $i = r, s$, are bifurcation points. In the following theorem, it will be formally shown that those points are saddle-node bifurcation points.

Theorem 2. *If $b_1 < b_1^*$, then the points (x_i, a_i), $i = r, l$, are local saddle-node bifurcation for the conservative system (5).*

Proof. In fact, it is enough that the following conditions are fulfilled, as shown in [21], Theorem 3.1, pp 84:

$$\begin{aligned} &A1\ \partial_{xx}F(x,a)|_{(x_i,a_i)} \neq 0, \\ &A2\ \partial_a F(x,a)|_{(x_i,a_i)} \neq 0. \end{aligned} \tag{12}$$

Indeed, we have $\partial_{xx}F(x,a)|_{x_l,a_l} > 0$ (resp., $\partial_{xx}F(x,a)|_{(x_r,a_r)} < 0$) because m has relative minimum (resp., maximum) in x_l (resp., x_r) and $\partial_a F(x,a)|_{(x_i,a_i)} = 1$. □

To summarize, the results obtained in Theorems 1 and 2 are illustrated in the bifurcation diagram of the conservative system associated with (5). In Figure 3(a), the red curve separates the region in terms of the parameters b_1 and b_2, for which the conservative system has a unique equilibrium (independent of the parameter a), of the region where the number of equilibrium solutions depends on the parameter a. In fact, if we take $(b_2, b_1) \in \mathbb{R}^2_+ - \{(b_2, b_1) \in \mathbb{R}^2_+ : b_1 \geq b_1^*\}$, then the conservative system may have one, two, or three equilibria as illustrated in Figure 3(b). In this figure, the solid lines are related to the stable equilibria, while the dotted line is related to the solutions of unstable equilibria. Furthermore, it can be shown that locally around the points (x_i, a_i), $i = l, r$, there is a saddle-node bifurcation.

3. Homoclinic Persistence

The discussion in this section is limited to the case $b_1 < b_1^*$ and $a \in]-m(x_r), -m(x_l)[$. The objective is to apply Melnikov's method to (5); when $f(t) = B\cos(\Omega t)$, it can be used to describe how the homoclinic orbits persist in the presence of the perturbation. For AFM models, the persistence of homoclinic orbits has great practical use since it can produce uncontrollable vibrations of the device, causing fail, and generate erroneous readings [9, 10, 15].

Before we address this problem, let us establish some notation. Consider the systems of the form

$$x' = f(x) + \varepsilon g(x,t), \quad x \in \mathbb{R}^2, \tag{13}$$

where f is a vector field Hamiltonian in $\mathbb{R}^2$, $g_i \in C^\infty(\mathbb{R}^2 \times \mathbb{R}/(T\mathbb{Z}))$, $i = 1, 2$, $g = (g_1, g_2)^T$, and $\varepsilon \geq 0$. Now, supposing in an unperturbed system, i.e., $\varepsilon = 0$in (13), the existence of a family of periodic orbits is given by

$$\gamma_e = \{(x_1, x_2) : E(x_1, x_2) = e\}, \quad e \in]\alpha, \beta[, \tag{14}$$

such that γ_e approaches a center as $e \longrightarrow \alpha$ and to an invariant curve denoted by γ_β as $e \longrightarrow \beta$. When γ_β is bounded, it is a homoclinic loop consisting of a saddle and a connection. We want to know if γ_β persists when (13), where $0 < \varepsilon \ll 1$, that is, if $\gamma_\beta(t, \varepsilon)$ is a homoclinic of (13) that is generated by γ_β. The first approximation of $\gamma_e(t, \varepsilon)$ is given by the zeros of Melnikov's function $M_e(t)$ which is defined as

$$M_e(t) := \int_{E(x_1,x_2)=e} g_2 dx_1 - g_1 dx_2. \tag{15}$$

Therefore, it is necessary to know the number of zeros of (7). For our purposes, the following theorem, which is an adaptation of [22], will be useful.

Theorem 3 ([22], **Theorem 6.4**). *Suppose $e_0 \in]\alpha, \beta]$ and $t_0 \in \mathbb{R}$.*

(1) If $M_{e_0}(t_0) \neq 0$, then there are no limit cycles near γ_{e_0} for $\varepsilon + |t_0 + t|$ which is sufficiently small

(2) If $M_{e_0}(t) = 0$ is a simple zero, then there is exactly one limit cycle $\gamma_{e_0}(t_0, \varepsilon)$ for $\varepsilon + |t_0 + t|$ which is sufficiently small that approaches γ_{e_0} when $(t, \varepsilon) \longrightarrow (t_0, 0)$

Remark 1. Melnikov's function can be interpreted as the first approximation in ε of the distance between the stable

and unstable manifold, measured along the direction perpendicular to the unperturbed connection; that is, $d(\varepsilon) \coloneqq \varepsilon(M_{\beta(t_0)}/f(\gamma_\beta)) + O(\varepsilon^2)$. In particular, when $M_\beta(t_0) > 0$ (resp., < 0), the unstable manifold is above (resp., below) the stable manifold (see [20, 23] for a detail discussion).

Rewriting (5) as a system of the form (13), we obtain

$$f(x_1, x_2) = \begin{pmatrix} x_2 \\ \\ m(x_1) + a \end{pmatrix},$$
$$g(x_1, x_2, t) = \begin{pmatrix} 0 \\ \\ B\cos(\Omega t) - \dfrac{C}{x_1^3} x_2 \end{pmatrix}. \tag{16}$$

From Theorem 1, we have that if $b_1 < b_1^*$ and $a \in]-m(x_r), -m(x_l)[$, the unperturbed system has three equilibria from which one is a saddle, denoted by $(x_{sa}, 0)$. The function's energy associated with the conservative system is given by (8) and homoclinic loops, denoted by Γ_l and Γ_r, and $E(x_1, x_2) = E(x_{sa}, 0) = \beta$.

When calculating Melnikov's function along the separatrix on the right Γ_r, the computation along Γ_l is identical; that is,

$$\begin{aligned} M_\beta(t_0) &= \int_{\Gamma_r} g_2 dx_1 - g_1 dx_2 = \oint_{\gamma_{\beta_r}} \left(E_{x_2} g_1 + E_{x_1} g_2\right) dt \\ &= \int_{-\infty}^{\infty} x_2(t) \left(B\cos(\Omega(t + t_0)) - \frac{C}{x_1^3(t)} x_2(t)\right) dt \\ &= B\cos(\Omega t_0) \int_{-\infty}^{\infty} \cos(\Omega t) x_2(t) dt \\ &\quad - B\,\mathrm{sen}(\Omega t_0) \int_{-\infty}^{\infty} \mathrm{sen}(\Omega t) x_2(t) dt - C \int_{-\infty}^{\infty} \frac{x_2^2(t)}{x_1^3(t)} dt \\ &= -2B\,\mathrm{sen}(\Omega t_0) \int_0^{\infty} \mathrm{sen}(\Omega t) x_2(t) dt - C \int_{-\infty}^{\infty} \frac{x_2^2(t)}{x_1^3(t)} dt. \end{aligned} \tag{17}$$

Note that

$$\int_{-\infty}^{\infty} \cos(\Omega t) x_2(t) dt = 0, \tag{18}$$

because $\cos(\Omega t) x_2(t)$ is an odd function. Consequently,

$$\begin{aligned} M_\beta(t_0) &= -2B\,\mathrm{sen}(\Omega t_0) \int_0^{\infty} \mathrm{sen}(\Omega t) x_2(t) dt \\ &\quad - C \int_{-\infty}^{\infty} \frac{x_2^2(t)}{x_1^3(t)} dt. \end{aligned} \tag{19}$$

By defining

Table 1: Properties of the case study of the AFM cantilever of Rützel et al. [24].

Symbol	Value
A_1	0.001×10^{-70} Jm^6
A_2	2.96×10^{-19} J
R	10 nm
K	0.87 N/m
Z_0	1.68108 nm

$$\begin{aligned} \xi_1 &= -2 \int_0^{\infty} \mathrm{sen}(\Omega t) x_2(t) dt, \\ \xi_2 &= -\int_{-\infty}^{\infty} \frac{x_2^2(t)}{x_1^3(t)} dt, \end{aligned} \tag{20}$$

we prove that ξ_1 and ξ_2 are bounded. Indeed, $dt = dx_1/x_1 = dx_1/x_2$ and $x_{sa} < x_1 < \overline{x}$ in Γ_r, where x_{sa} and $\overline{x}$ are consecutive zeros of $E(x_1, 0) - \beta$. Now if $E(x_1, x_2) = \beta$, then

$$x_2^2 = 2\left(\beta + a x_1 + \frac{b_2}{x_1} - \frac{b_1}{7x_1^7} - \frac{x_1^2}{2}\right). \tag{21}$$

Hence,

$$\xi_1 \le 2 \int_0^{\infty} x_2(t) dt = 2 \int_{x_{sa}}^{\overline{x}} dx_1 = 2(\overline{x} - x_{sa}). \tag{22}$$

On the contrary,

$$\begin{aligned} |\xi_2| &\le 2C \int_{x_{sa}}^{\overline{x}} \left|\frac{x_2}{x_1^3}\right| dx_1 \\ &= 2C \int_{x_{sa}}^{\overline{x}} \frac{\sqrt{2(\beta + a x_1 + (b_2/x_1) - (b_1/7x_1^7) - (x_1^2/2))}}{|x_1^3|} dx_1 < \infty. \end{aligned} \tag{23}$$

Finally, Melnikov's function is rewritten as

$$M_\beta(t_0) = B\,\xi_1\,\mathrm{sen}(\Omega t_0) + C\,\xi_2. \tag{24}$$

Theorem 4. *Under the conditions of item 2 of Theorem 1, we have that the homoclinic orbits of (5) persist as long as ε is sufficiently small and*

$$\frac{B}{C} > \left|\frac{\xi_2}{\xi_1}\right|. \tag{25}$$

Proof. Condition (25) implies that Melnikov's function (24) has a simple zero. Consequently, Theorem 3 reaches the desired conclusion.

Example 1. For illustrative purposes, we have taken from [24] the realistic values of the physical parameters in Table 1. The values in Table 1 are related to the following adimensionalized values b_1, b_2, and a:

$$b_1 = \frac{113876}{10000000},$$
$$b_2 = \frac{148148}{1000000},$$
$$a = 1.07468, \tag{26}$$
$$|\xi_1| = 0.290315,$$
$$|\xi_2| = 0.382056.$$

For instance, fix $C = 1$ and $\Omega = 1$, and Theorem 4 guarantees that if $B > 1.316$, then the homoclinic persists.

Data Availability

The data used to support the findings of this study are included within the article.

Conflicts of Interest

The authors declare that they have no conflicts of interest.

Acknowledgments

The authors have been financially supported by the Convocatoria Interna UTP 2016 (project CIE 3-17-4).

References

[1] C. F. Ziborov and G. Binning, "Atomic force microscope," *Physical Review Letters*, vol. 56, no. 9, pp. 930–934, 1986.

[2] van de B. Bram, A. Farbod, and K. G. Murali, "Experimental setup for dynamic analysis of micro-and nano-mechanical systems in vacuum, gas and liquid," *Micromachines*, vol. 10, no. 3, p. 162, 2019.

[3] C. K. Chua, W. Y. Yeong, and J. An, "3D printing and bioprinting in MEMS technology," *Micromachines*, vol. 8, no. 7, p. 229, 2017.

[4] S. Morita, F. Giessibl, E. Meyer et al., *Noncontact Atomic Force Microscopy*, Springer, New York, NY, USA, 2015.

[5] R. Bowen and N. Hilal, *Atomic Force Microscopy in Process Engineering: Introduction to AFM for Improved Processes and Products*, Elsevier, Amsterdam, Netherlands, 2009.

[6] B. Bhushan and O. Marti, *Nanotecnology, Scanning Probe Microscopy-Principle of Operation, Instrumentation, and Probes*, Springer, Berlin, Heidelberg, 2010.

[7] T. Pleshakova, A. Kaysheva, I. Shumov et al., "Detection of hepatitis C virus core protein in serum using aptamer-functionalized AFM chips," *Micromachines*, vol. 10, no. 2, p. 129, 2019.

[8] A. L Rachlin and G. S Henderson, "An atomic microscope (AFM) study of the calcite cleavage plane: image averaging in fourier space," *American Mineralogist*, vol. 77, pp. 904–910, 1992.

[9] M. Ashhab, V. Salapaka, M. Dahleh et al., "Control of chaos in atomic force microscopes," in *Proceedings of the American Control Conference*, pp. 196–202, Albuquerque, NM , USA, June 1997.

[10] M. Ashhab, V. Salapaka, M. Dahleh et al., "Melnikov-based dynamical analysis of microcantilevers in scanning probe micrsoscopy," *Nonlinear Dynamics*, vol. 20, pp. 197–229, 1999.

[11] F. Jensen, *Introduction to Computational Chemestry*, John Wiley & Sons, Hoboken, NJ, USA, 2007.

[12] J. E. Lennard-Jones, "On the determination of molecular field," *Proceedings of the Royal Society A: Mathematical, Physical and Engineering Sciences*, vol. 106, no. 738, pp. 441–462, 1924.

[13] S. G. Brush, "Interatomic forces and gas theory from Newton to Lennard-Jones," *Archive for Rational Mechanics and Analysis*, vol. 39, no. 1, pp. 1–29, 1970.

[14] M. I. Younis, *MEMS Linear and Nonlinear Statics and Dynamics*, Springer, Berlin, Heidelberg, 2011.

[15] W. M. Zhang, G. Meng, J. B. Zhou et al., "Nonlinear dynamics and chaos of microcantilever-based TM-AFMs with squeeze film damping effects," *Sensors*, vol. 9, pp. 3854–3874, 2009.

[16] F. Huber and F. Giessibl, "Low noise current preamplifier for qPlus sensor deflection signal detection in atomic force microscopy at room and low temperatures," *Review of Scientific Instruments*, vol. 88, no. 7, article 073702, 2017.

[17] M. Babak and A. G. Aristides, "Compensation of scanner creep and hysteresis for AFM nanomanipulation," *IEEE Transactions on Automation Science and Engineering*, vol. 5, no. 2, pp. 197–206, 2008.

[18] Y. Zhang, Y. Fang, X. Zhou, and X. Dong, "Image-based hysteresis modeling and compensation for an AFM piezoscanner," *Asian Journal of Control*, vol. 11, no. 2, pp. 166–174, 2009.

[19] A. A. Andronov, E. A. Leontovich, I. I. Gordon et al., *Qualitative Theory of Second-Order Dynamical Systems*, John Wiley & Sons, New York, NY, USA, 1973.

[20] L. Perko, *Differential Equations and Dynamical Systems*, Springer, Berlin, Heidelberg, 3rd edition, 2000.

[21] Y. Kuznetsov, "Elements of applied bifurcation theory," in *Applied Mathematical Sciences*, Springer, Berlin, Heidelberg, 3rd edition, 2004.

[22] M. Han and P. Yu, *Normal Forms, Melnikov Functions, and Bifurcations of Limit Cycles*, Springer, Berlin, Heidelberg, 2012.

[23] J. Guckenheimer and P. Holmes, *Nonlinear Oscillations, Dynamical Systems, and Bifurcations of Vector Fields*, Springer, Berlin, Heidelberg, 1986.

[24] S. Rützel, S. I. Lee, and A. Raman, "Nonlinear dynamics of atomic-force-microscope probes driven in Lennard-Jones potentials," *Proceedings of the Royal Society of London. Series A: Mathematical, Physical and Engineering Sciences*, vol. 459, no. 2036, pp. 1925–1948, 2003.